Visualized Degradation of Poly(alkynoate)s toward Diols and Structure Controlled Multifunctional *N*-Heterocyclic Compounds

Bo Song,[†] Tianwen Bai,[§] Dongming Liu,[†] Rong Hu,[†] Dan Lu,[†] Anjun Qin,*[†] Jun Ling,*[§] Ben Zhong Tang*[†,‡]

[†] State Key Laboratory of Luminescent Materials and Devices, Guangdong Provincial Key Laboratory of Luminescence from Molecular Aggregates, SCUT-HKUST Joint Research Institute, AIE Institute, Center for Aggregation-Induced Emission, South China University of Technology (SCUT), Guangzhou 510640, China

[‡] Department of Chemistry, Hong Kong Branch of Chinese National Engineering Research Centre for Tissue Restoration and Reconstruction, Institute for Advanced Study, and Department of Chemical and Biological Engineering, The Hong Kong University of Science & Technology (HKUST), Clear Water Bay, Kowloon, Hong Kong, China.

[§] MOE Key Laboratory of Macromolecular Synthesis and Functionalization, Department of Polymer Science and Engineering, Zhejiang University, Hangzhou 310027, China

ABSTRACT: Degradable polymers are highly desirable due to the tremendous growth of polymer wastes. Some polymers could be degraded under strong acidic or basic conditions toward unknown or unvalued products (*i.e.* downcycling). New methods to degrade polymers into monomers or high-value-added materials (*i.e.* upcycling) are more preferred for sustainable developments. In this work, linear and cross-linked poly(alkynoate)s were successfully degraded by benzamidine with 100% conversion into not only diols, a kind of monomers, but also high-value-added *N*-heterocyclic compounds of pyrimidone and imidazolone derivatives in high yields through controlling the reaction conditions. Notably, thanks to the AIE feature of the degraded products, the degradation process could be visualized under UV light via gradually increased luminescent intensity of the reaction mixtures, which facilitates the monitoring of the polymer degradation. Using this highly efficient degradation reaction, fluorescence patterns could be generated through microcontact printing (μCP) of the stamp on the thin films of poly(alkynoate)s. Moreover, the pyrimidone derivatives could be applied in bioimaging and inhibiting bacteria, and the imidazolone derivatives could be used for the detection and recovery of gold (III) ions from electronic waste and serve as the fluorescent sensor to detect *in situ* generated amines from food spoilage. Thus, this work presents a visualized and high value product-selective degradation to solve the end-of-life issue of polymers.

INTRODUCTION

Steeply increased synthetic polymeric materials are designed and synthesized nowadays, not only serving as plastics, rubbers and fibers, but also being used for organic light emitting diodes (OLED), organic photovoltaics, biomedical materials, etc.[1-5] However, these polymeric materials are predominantly based on petroleum resources and designed for superior performance, and the degradability and recyclability are ignored, which has led to tremendous growth of polymer wastes. Contaminated polymer wastes are now ubiquitous on the earth, including freshwater systems, terrestrial habitats, and all major ocean basins, affecting human beings deeply.[6,7] Undoubtedly, developing new degradable polymeric materials and new methods for polymer degradation to solve the end-of-life issue of polymers are highly desirable.

Various degradable polymers appeared over the past few decades by the incorporation of reactive groups, which can be cleaved under appropriate conditions.[8-10] However, most of them suffer from one or more of the following issues, such as slow degradation rate, incomplete degradation, unknown or unvalued degraded products. (Figure 1).[11] In recent years, Chen, Hong, Lu, Moore, Hillmyer, and Li groups have developed a series of chemically recyclable polymers which could be depolymerized to monomers under certain conditions, respectively.[12-17] These works are groundbreaking in solving the

end-of-life issue of polymers. However, there are still some issues to be addressed in their developed polymers. For example, the abilities of polymerization and depolymerization are opposite each other, in other words, one of the processes is more efficient to take place while the other is less efficient. Thus, balancing the depolymerizability polymers and their properties is difficult. What is more, the depolymerization of some polymers needs catalysts or harsh reaction condition, such as elevated temperature up to 300 ºC, which might hamper their practical applications.

Polyester is a large class of significant synthetic polymers, which is widely used as engineering plastics, textile fibers, adhesives, etc. Poly(alkynoate)s are an emerging kind of unsaturated polyester, which contains both ester and ethynyl groups in the main chains.[18-21] They are generated from the renewable monomer CO_2, so they could be regarded as a kind of sustainable polymers. Poly(alkynoate)s possess excellent solubility and good thermostability. They could be degraded in the strong basic conditions, but it is an incomplete process toward unknown and unvalued products (*i.e.* downcycling).[18] Thus, a new controllable degradation method for poly(alkynoate)s is highly desired. Considering that ethyl phenylpropiolate could react with benzamidine to generate *N*-heterocyclic compounds and ethanol,[22,23] we envisaged using
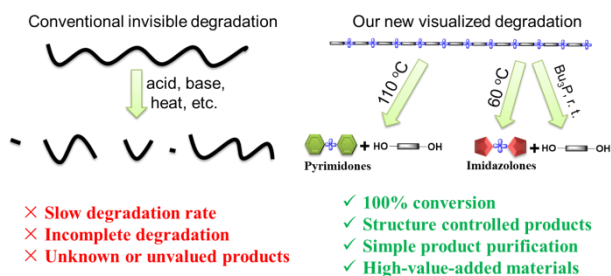
Figure 1. Schematic comparisons between conventional and our new degradation method

this addition−heterocyclization−cleavage reaction to degrade poly(alkynoate)s in a repurposing process (*i.e.* upcycling) (Figure 1).

Indeed, poly(alkynoate) P1 could successfully be degraded by adding benzamidine with 100% conversion into diols and high-value-added *N*-heterocyclic compounds, among which pyrimidone derivatives were obtained at 110 °C (Figure 2, Path A) while imidazolone derivatives were obtained at 60 °C (Figure 2, Path B) or at room temperature upon addition of the catalyst of Bu_3P (Figure 2, Path C). Thermoset poly(alkynoate) P2 was also successfully degraded to imidazolone derivatives. *In situ* Fourier transform infrared (FT-IR) spectroscopy and density functional theory (DFT) calculation well revealed the reaction kinetics and mechanism. Notably, thanks to the emissive property of the degraded compounds, the degradation process could be visualized under UV light via gradually increased luminescent intensity of the reaction mixtures and also could be introduced into microcontact printing to generate fluorescence patterns. The *N*-heterocyclic compounds obtained from P1 possess unique AIE characteristics and could be applied in diverse areas.

RESULTS AND DISCUSSION

Reaction Condition-Orientated Degradation of Poly(alkynoate)s. The poly(alkynoate)s P1 containing both ester and ethynyl groups in the main chains was synthesized via the Ag_2WO_4-catalyzed three component polymerization of CO_2, diyne 1, and alkyl dihalide 2 according to our previously reported procedures.[18] Its structure was unambiguously confirmed by nuclear magnetic resonance (NMR) spectroscopies.

In order to achieve product-selective degradation of poly(alkynoate)s via benzamidine 3 to obtain *N*-heterocyclic compounds 4 and 5, the model reactions of 3 and 6 carried out at different temperatures were first investigated (Table S1). The results showed that only a pyrimidone derivative 7 was obtained at 110 °C while an imidazolone derivative 8 was obtained at 60 °C. Interestingly, within these two temperatures, a mixture of 7 and 8 were obtained. When Bu_3P was used as the catalyst, only 8 was obtained no matter what temperature is (Table S2). These results demonstrated a reaction conditions orientation. The structures of 7 and 8 were confirmed via NMR spectroscopies and single crystal X-ray diffraction patterns (Figure S1-S3, CCDC 1916544 and 1916517).

Encouraged by the results of the model reaction, the degradation of P1 was investigated. When P1 reacted with 3 in toluene at 110 °C for 12 h, a yellow precipitate of pyrimidone derivative 4 was obtained after simple filtration and 1,8-octanediol was also yielded via the concentration of the filtered solution. The total yield of pyrimidone derivative 4 and

1,8-octanediol is 92% (Figure 2, Path A). However, when P1 reacted with 3 in toluene at 60 °C for 12 h, the orange precipitate of imidazolone derivative 5 and 1,8-octanediol were obtained via the same operation as the path A with the total yield of 90% (Figure 2, Path B). Interestingly, when a catalytic amount of Bu_3P was added, the degradation of P1 could be carried out at room temperature and the same degraded products as path B were obtained with the total yield of 94% (Figure 2, Path C). The GPC analysis of the degradation process showed the gradual shift of the peaks to the late elution time. Only a narrow single peak could be observed after 8 h, confirming a complete degradation of P1 (Figure 3A).

The structures of the degraded products were characterized by FT-IR spectroscopy and ^{1}H and ^{13}C NMR spectroscopies, and satisfactory structural analysis data were obtained. The FT-IR spectra of P1, and degraded products 4 and 5 provided in Figure 3B-D showed that the C≡C stretching vibrations at 2211 cm^{-1} in the spectrum of P1 could not be observed in the spectra of 4 and 5. Meanwhile, the absorption bands of P1, 4 and 5 associated with C=O stretching vibrations could be observed at 1710, 1651 and 1701 cm^{-1}, respectively. To facilitate the structural characterization, another model reaction of 9 and 3 was carried out to prepare model compounds 4-1 and 5-1 (Scheme S1). As shown in ^{1}H NMR spectra (Figure 3E-H), the *N*-H protons of 4 and 5 resonated at 12.71 and 12.07 ppm, respectively. Meanwhile, the ethynyl protons of 4 and 5 resonated at 6.85 and 6.92 ppm, respectively. Notably, The ^{1}H NMR spectra of degraded products 4 and 5 obtained from P1 are almost the same as these of model compounds 4-1 and 5-1, and the ^{1}H NMR spectrum of 1,8-octanediol obtained from P1 is also almost the same as that of the standard sample (Figure S4), confirming the structures of the degraded products.

After achieving a complete degradation of soluble linear poly(alkynoate)s, we challenged to degrade insoluble thermoset poly(alkynoate)s. It is well known that thermoset materials have favorable material properties but are unable to reprocess and are difficult to recycle due to their chemically cross-linked structures.[24] To tackle this difficulty with our strategies, an insoluble cross-linked polymer P2 was synthesized from the Ag_2WO_4-catalyzed polymerization of tetrayne (10), alkyl dihalide (2) and CO_2 under mild reaction conditions (Scheme S2), which could not be dissolved in any solvent. As shown in Scheme S3, when benzamidine 3 and Bu_3P were added into the suspension of P2 in tetrahydrofuran (THF), the polymer disappeared and the reaction mixtures became an orange solution at as short as 10 min, and the degraded products 11 and 1,8-octanediol were obtained.

Kinetics and Mechanism Investigation. To better understand the kinetic profile of the degradation, *In situ* FT-IR spectroscopy was used to monitor the degradation process. When the degradation of P1 was carried out at 110 °C with 1 equiv 3 relative to the number of alkynoates moiety, a new absorption band attributed to the C=O stretching vibration of 4 emerged at 1652 cm^{-1}, which intensity increased over 30 min but remained almost unchanged afterward, indicating the degradation could be finished in 30 min (Figure 4A). When the degradation of P1 was carried out at 110 °C with 1 equiv 3 and 0.2 equiv Bu_3P, a new absorption band attributed to the C=O stretching vibration of 5 appeared at 1701 cm^{-1}, which increased rapidly to reach saturation after 5 min, suggestive of the fast rate and high efficiency of the degradation upon adding the catalyst Bu_3P (Figure 4B). The investigation of the
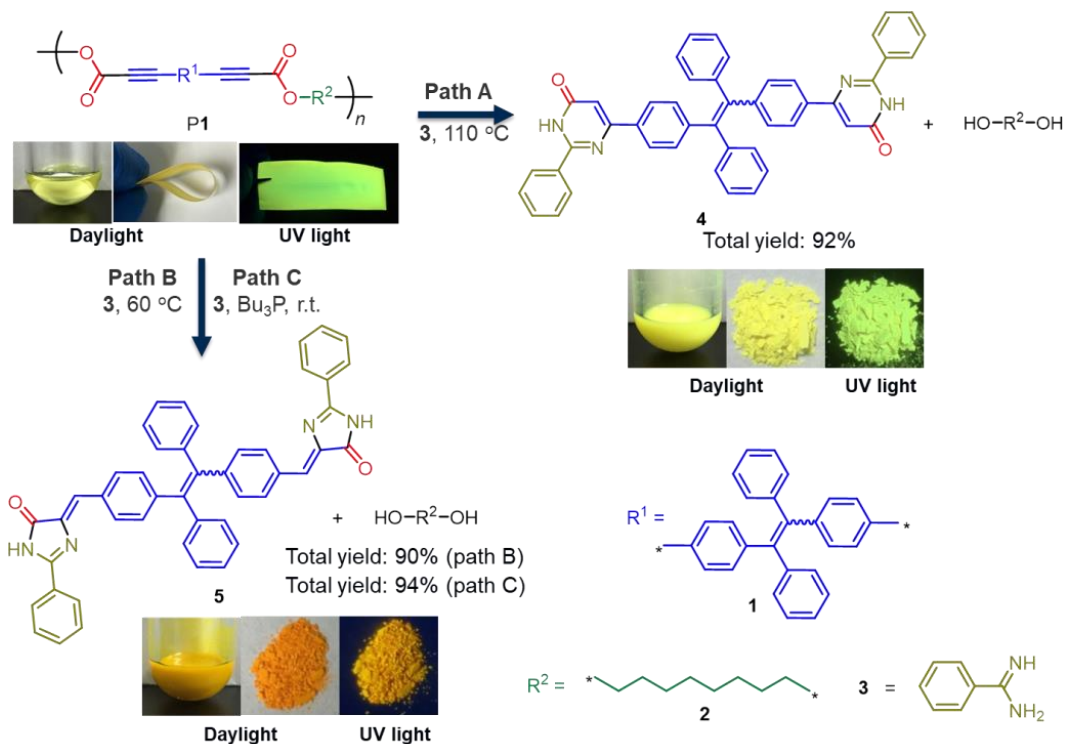
Figure 2. Product-selective degradation of **P1** toward diols and *N*-heterocyclic compounds
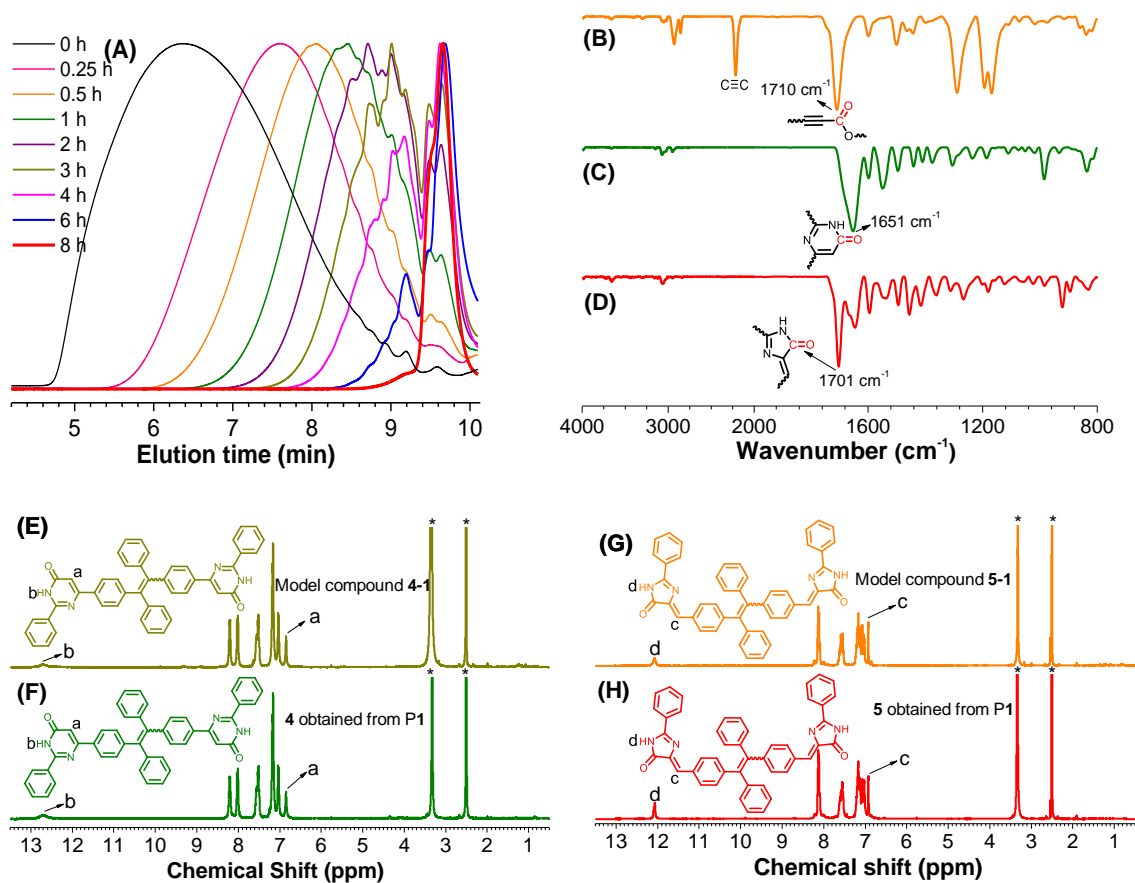

Figure 3. (A) Overlay of the GPC curves at different degradation times (condition: 60 °C, [**P1**] = [**3**] = 0.1 M), FT-IR spectra of (B) **P1**, (C) **4** and (D) **5**. [^1]H NMR spectra of (E) model compound **4-1**, (F) recycled **4** from **P1**, (G) model compound **5-1**, and (H) recycled **5** from **P1** in dimethyl sulfoxide (DMSO)-d_6. The solvent peaks are marked with asterisks.
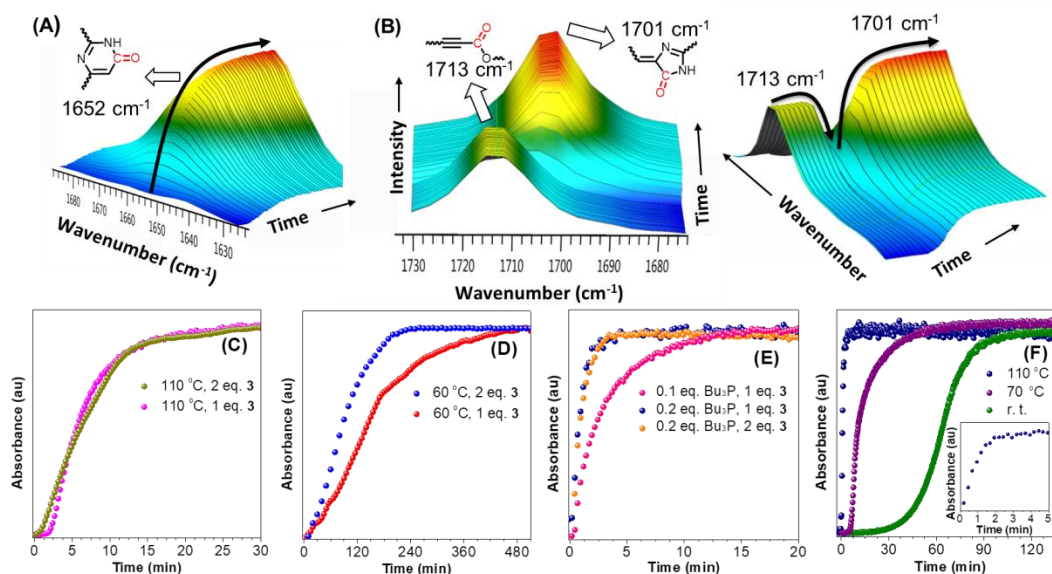
Figure 4. Three-dimensional Fourier transform IR profiles of the peaks (A) at 1652 cm^{-1} for the degradation at 110 °C with 1 equiv **3**, (B) at 1713, 1701 cm^{-1} for the degradation at 110 °C with 1 equiv **3** and 0.2 equiv Bu$_3$P. (C, D) The time-dependent peak intensity at 1652 cm^{-1} (110 °C) or at 1701 cm^{-1} (60 °C) with different equivalent of **3**, (E) The time-dependent peak intensity at 1701 cm^{-1} with different equivalent of **3** and Bu$_3$P at 110 °C. (F) The time-dependent peak intensity at 1701 cm^{-1} with 1 equiv **3** and 0.2 equiv Bu$_3$P at different temperatures.

effect of temperature, the molar ratio of **3** and Bu$_3$P on the degradation suggested that the molar ratio of **3** almost could not affect the degradation rate at 110 °C, but it exerted significant effect at 60 °C during the degradation (Figure 4C and 4D). When 2 instead of 1 equiv **3** was added into the reaction mixtures at 60 °C, the degradation time could be shortened from 500 to 250 min. When Bu$_3$P was used to promote the degradation, its molar ratio affected the degradation rate significantly. The degradation time was extended from 5 to 15 min with the molar ratio of Bu$_3$P decreasing from 0.2 to 0.1 equiv (Figure 4E). Moreover, the degradation of **P1** could also be finished at room temperature for only 2 h in the presence of Bu$_3$P (Figure 4F). The ^{1}H NMR spectra of original unseparated reaction mixtures at different degradation conditions indicated that the resonance peak representing the protons of methylene group adjacent to the ester groups in **P1** was totally disappeared after the degradation (Figure S5), indicating nearly 100% conversions of **P1**.

Moreover, the theoretical calculation was employed to have a deep understanding of above degradation behaviors. We used ethyl phenylpropiolate **6** and benzamidine **3** as model reagents to simplify the calculation and employed DFT to analyze the mechanism of three paths of the degradation.

As shown in Figure 5, for path A, three steps were observed, *i.e.* nucleophilic addition, nitrogen-activated double bond rotation, and carbonyl addition. First, the ethynyl group was attacked by **3** and formed **A_3** via the proton transfer process. This nucleophilic addition was only allowed in *E*-configuration due to the steric hindrance of ester group. After a typical nitrogen-activated double bond rotation (**A_TS3**), the ester group was attacked by amidine group (**A_TS4**). After leaving equivalent ethanol, the product (**A_6**) was yielded with a quite low ΔG = -42.9 kcal/mol. The highest energy barrier was confirmed at the step of nitrogen-activated double

bond rotation with ΔG$_A$ = 44.0 kcal/mol, which is the rate determining step. Thus, the molar ratio of **3** would not affect the degradation rate at 110 °C, which agreed well with our *in situ* FT-IR results (Figure 4C).

In path B, only two main steps were observed, *i.e.* electrophilic addition and carbonyl addition (Figure 5). The ethynyl group was attacked by **3** at the ester side firstly. After a similar proton transfer process (**B_TS2**), the ester group was attacked by amidine group to form a five-membered ring (**B_TS4**) and produce **B_5** with ΔG = -32.1 kcal/mol. The highest energy barrier shifted to the step of electrophilic addition with **3** with ΔG$_B$ = 40.6 kcal/mol, due to the absence of nitrogen-activated double bond rotation. Accordingly, the molar ratio of **3** would affect the degradation rate significantly at 60 °C. This conclusion is also consistent with our *in situ* FT-IR results (Figure 4D).

For the comparison of paths A and B, the latter was observed with lower ΔG$_B$ (40.6 kcal/mol) than that of path A (ΔG$_A$ =44.0 kcal/mol), but with a more unstable product (**B_5**: -32.1 kcal/mol) than that of path A (**A_6**: -42.9 kcal/mol). The constant (*k*) of reaction rate is an important parameter for a chemical reaction. According to Rice–Ramsperger–Kassel–Marcus (RRKM) theory,[25] *k* can be calculated from ΔG‡ according to Equation (1) and the quotients are obtained from ΔΔG‡ according to Equation (2).

$$k = A\exp(-\frac{\Delta G^{\ddagger}}{RT}) \quad (1)$$

$$\frac{k_2}{k_1} = A\exp(-\frac{\Delta G_2^{\ddagger} - \Delta G_1^{\ddagger}}{RT}) = \exp(\frac{\Delta\Delta G_{12}^{\ddagger}}{RT}) \quad (2)$$

where *A* is a constant, *R* is the ideal gas constant (8.314 J·mol^{-1}·K^{-1}), and *T* is 298.15 K. Therefore, k_B/k_A could be deduced as
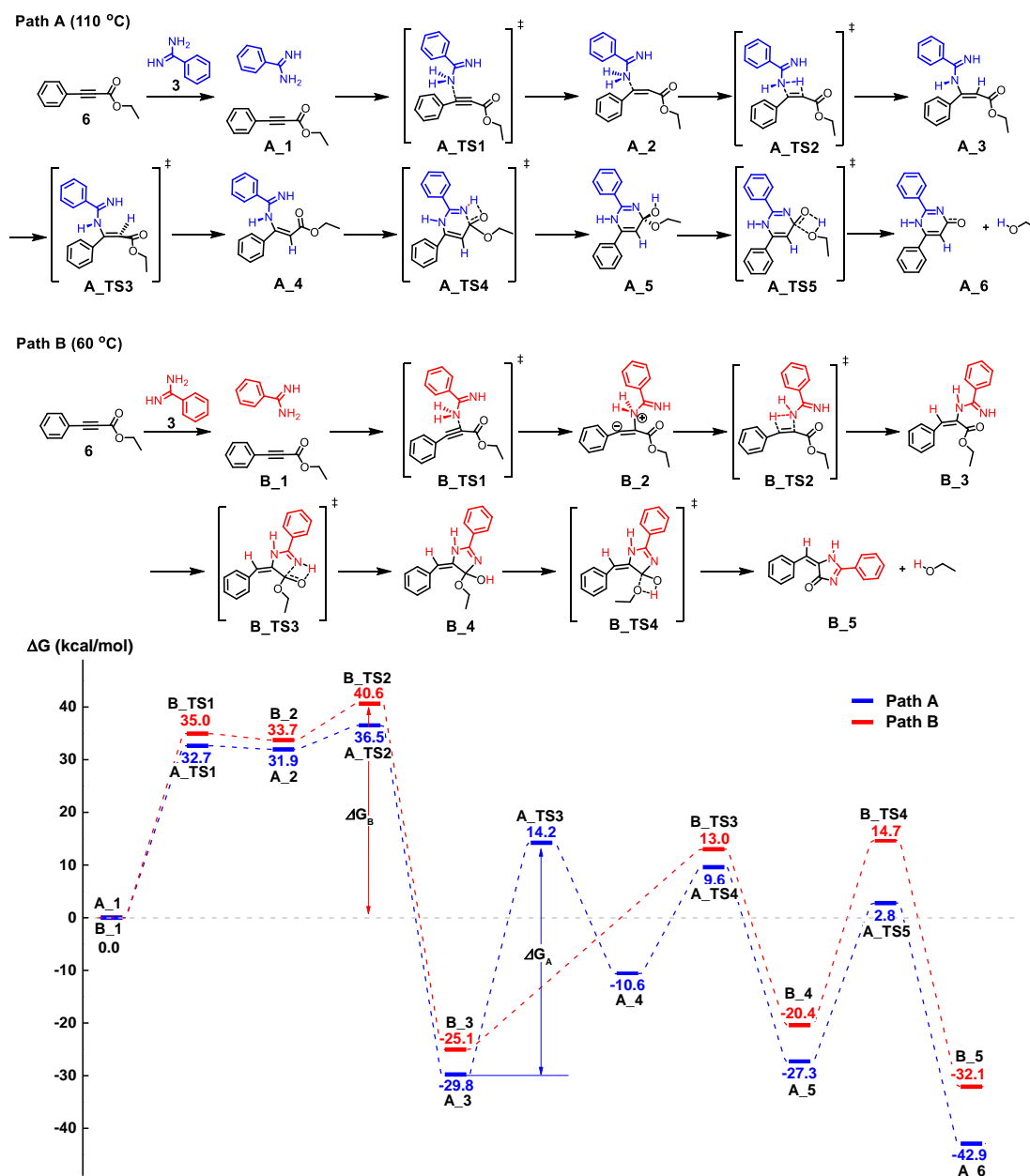
Figure 5. DFT-calculated profiles of the path A (blue) and path B (red). All numbers are given as relative Gibbs free energy (kcal/mol)

3×10^2, which indicated that only path B could occur under low temperature. Meanwhile, path A is favored at high temperature with a more stable product (Figure 5).

Because PMe$_3$ showed the same effect as PBu$_3$ on the degradation,[22,23] the former was used as a model catalyst to simplify the calculation (Scheme S4). The ethynyl group was firstly attacked by PMe$_3$ to produce a compound **C_2**, which processed similar electrophilic addition with **3**. Then **C_5** was yielded after proton transfer. Cleaving PMe$_3$ could either occur before (**C_TS4_L**) or after (**C_TS6_As**) carbonyl addition. Since the very high energy barrier on **C_TS4_As** step (60.7 kcal/mol), PMe$_3$ could only be cleaved before carbonyl addition (**C_TS4_L**). Thus **C_6_L** shared the same reaction process as the path B (**B_3** to **B_5**) (Figure S6). Apparently, PMe$_3$ could greatly reduce the energy barrier compared with path B,

the reaction rate was increased immensely, which was also consistent with our *in situ* FT-IR results (Figure 4E and F).

Photophysical properties of Degraded Products. Because **4** and **5** contain tetraphenylethene (TPE), a typical moiety featuring aggregation-induced emission (AIE) characteristics,[26-28] their emission behaviors were systematically investigated in DMSO/water and THF/water mixtures with different water fractions (f_w, Figures S7 and 8), respectively, and their absolute photoluminescence (PL) quantum yields (Φ_F) were also tested (Table S3). The results showed that both of them are AIE-active and follow the mechanism of the restriction of intramolecular motion (RIM).[26] They emitted faintly in solutions, but adding a poor solvent like water greatly enhanced
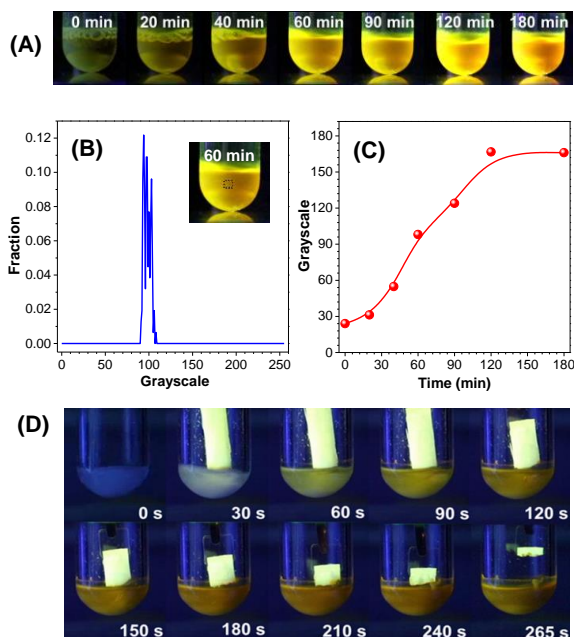
Figure 6. (A) Fluorescence images of the reaction mixture at different times. (B) Grayscale distribution of the selected area at 60 min. Inset: fluorescence image of the reaction mixture at 60 min and the selected area for grayscale analysis. (C) Plot of time against grayscale of the reaction mixture. (D) Photographs of the film of P**1** before and after degradation.

the emission intensity. The highest emission values were recorded in the DMSO/water mixtures with f_w values of 60% for **4** and in THF/water mixtures with f_w values of 90% for **5**, Moreover, the Φ_F of **4** in its film state is measured to be 78.2%, which is much higher than that of **5** (20.7%) due to highly twisted molecular conformation of **4** that hampers the intermolecular π-π stacking interaction in the solid state, suppressing non-radiative transition and activating radiative one.

***In Situ* Visualization of Degradation Process.** Thanks to their faint emission in the solution and intense luminescence in the aggregated state, the AIE luminogens (AIEgens) have been successfully used to directly visualize invisible things before, such as defects,[29] crystallization process,[30] the glass-transition temperature (T_g),[31] and polymerization process.[32] However, direct visualization of the degradation process of a polymer using AIE technology is virtually unexplored.

Since its degraded product **5** enjoys the AIE feature, herein, the degradation of P**1** was visualized for the first time. As shown in Figure 6A, the degradation of P**1** with **3** and Bu$_3$P at room temperature was performed under UV light. The reaction mixture initially showed almost no emission. Then orange luminescence was observed and enhanced gradually with the extension of time. The reason is that the AIE-active degraded product **5** was precipitated continuously during the degradation, which emits intensively in the aggregate state. The fluorescence in the middle part of tube was analyzed at different interval by ImageJ software, in which, grayscale was automatically calculated at each pixel to represent the brightness or intensity of fluorescence signal.[33] Accordingly, the statistical distribution and average value of grayscale of the selected area were obtained. Figure 6B demonstrated the results at 60 min as an example. The plot of grayscale versus time shown in Figure 6C gives a positive correlation. The highest value of
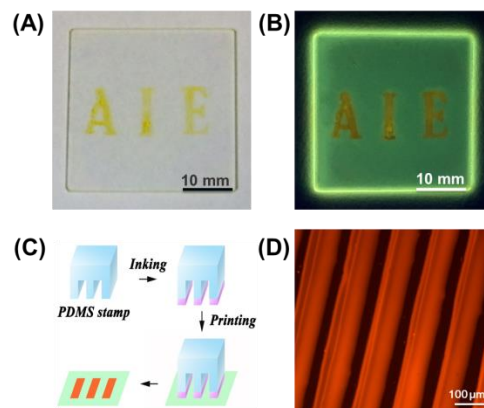

Figure 7. (A and B) Two-dimensional patterns generated by the degradation of P**1** film taken under daylight and UV light, respectively. Excitation wavelength: 365 nm. (C) Illustration of μCP and (D) Fluorescence microscopy image after μCP. Excitation wavelength: 540-552 nm. Emission wavelength: 575-640 nm.

grayscale appeared at 120 min and then reached saturation, and its shape was similar to that of the *in situ* FT-IR curve (Figure 4F), indicating that *in situ* visualization of the degradation process via AIE technology is reliable. Moreover, the degradation process could also be visualized under UV light with a P**1** film slowly immersing into the toluene solution of **3** and Bu$_3$P at room temperature (Figure 6D).

Microcontact Printing. As aforementioned, the Bu$_3$P-catalyzed degradation of P**1** is very fast at room temperature with the fluorescence color change, it is an ideal candidate to be applied in microcontact printing (μCP) to generate fluorescence patterns. μCP as a kind of soft lithography possesses many advantages including high resolution, very short reaction times, simple large-area patterning, and low cost, etc.[34,35] Certainly, it can solve the disadvantages encountered in microfabrication, which is the basic technology used for making all microelectronic systems, such as high cost, complex facilities and technologies for high-energy radiation needed and limitation to extremely flat silicon substrates. μCP allows the patterned transfer of a molecular ink onto a surface using an elastomeric stamp. Several reactions such as Cu(I)-catalyzed azide–alkyne coupling (CuAAC), Diels-Alder reaction, thiol-ene and amino-yne click reactions have been introduced into μCP.[36,37].

Herein, the Bu$_3$P-catalyzed degradation was applied in this area. First, the thin films of P**1** on quartz substrates (30×30 mm) were prepared via spin coating. Then a stamp with "AIE" characters was incubated with the ink, *i.e.* the toluene solution of **3** and Bu$_3$P and placed on the prepared polymer films. Only after 2 min, an orange "AIE" pattern was obtained under both daylight and UV light which represented the generation of degraded product **5** (Figure 7A and B).

Encouraged by above results, poly(dimethylsiloxane) (PDMS) was used as the elastomeric stamp for μCP. As shown in Figure 7C, the PDMS stamp with micron-scale pattern was also inked and printed on the prepared polymer films. Then the fluorescence microscopy photos were taken by fluorescence microscope after 2 min. The well-resolved two-dimensional fluorescence pattern was thus generated (Figure 7D), indicating that the degradation process showed great potential for μCP.
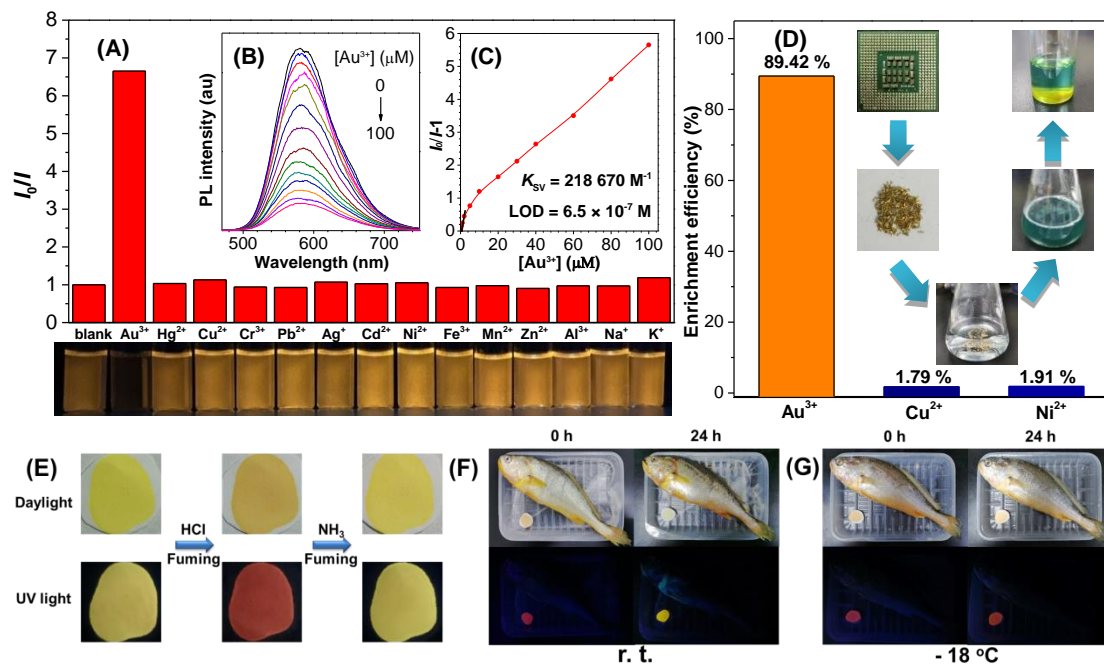
Figure 8. (A) Fluorescence detection of gold ion with *N*-heterocyclic compound **5**. Relative intensity (I_0/I) at 578 nm of **5** in THF/H$_2$O mixture (v/v, 1/9, 10 μM) in the presence of different metal ions (100 μM) and the corresponding fluorescence photos taken under UV irradiation, I_0 = PL intensity in the absence of metal ions. (B) PL spectra of **5** in THF/H$_2$O mixture (v/v, 1/9, 10 μM) containing different amounts of Au^{3+}. (C) Stern-Volmer plot of relative intensity (I_0/I-1) of **5** in THF/H$_2$O mixture (v/v, 1/9, 10 μM) versus [Au^{3+}]. I_0 = PL intensity in the absence of Au^{3+}. Excitation wavelength: 365 nm. (D) The selective extraction of Au^{3+} by **5** from the leaching solution of a discarded CPU. (E) Photographs of **5** on the filter paper via HCl and NH$_3$ fuming under daylight and UV light. Excitation wavelength: 365 nm. (F, G) Spoilage detection of fishes in packages for 24 h at room temperature or -18 °C using the test strips of protonated **5**.

High-Value-added Products. The *N*-heterocyclic compounds **4** and **5** obtained from **P1** possess unique AIE features and could be applied in diverse areas. Compound **4** is a kind of pyrimidine derivatives, which are well-known with good pharmacological activity and have potentials as antibacterial agents *etc*.[38-40] Thereof, the antibacterial property of **4** was investigated. First, the confocal laser scanning microscopy (CLSM) images of **4** incubated with Gram-positive bacterium *S. aureus* and Gram-negative bacterium *E. coli* for 20 min suggested that **4** was located around *S. aureus* quickly, while no interaction was between **4** and *E. coli* (Figure S9).Therefore, the *in vitro* antibacterial activity using *S. aureus* as the representative was studied. As shown in Figure S10, the standard plate counting results showed that the growth of *S. aureus* could be inhibited effectively with nearly 90% inhibition ratio, which indicated that the degraded product **4** has great potential for the imaging and inhibition of bacteria.

Moreover, **5** is a kind of imidazolone derivatives, which are well-known ligands for gold (III) ions with strong binding.[41] Thus, **5** might be useful to detect and recover Au(III) ions from electronic waste, which is of great economic benefit, considering that the Au content of discarded PCs and mobile phones (280 g/ton) is much higher than that from gold ore (5 g/ton).[42-46] The THF/water mixture of **5** with 90 vol% water fraction was selected to detect Au^{3+} owing to its highest PL intensity. Meanwhile, a large variety of metal ions including Hg^{2+}, Cu^{2+}, Cr^{3+}, Pb^{2+}, Ag$^+$, Cd^{2+}, Ni^{2+}, Fe^{3+}, Mn^{2+}, Zn^{2+}, Al^{3+}, Na$^+$, and K$^+$ were also tested with the same aqueous mixture of **5**. The results showed that only Au^{3+} exhibits dramatic fluorescence quenching due to the formation of **5**-Au^{3+} complexes,

and negligible change on PL intensity and fluorescence image was observed for the other metal ions, indicating high specificity of Au(III) detection (Figure 8A). Next, the sensitivity of Au(III) detection was investigated via the addition of Au^{3+} into the THF/water mixture of **5** from 0 to 100 μM. The PL intensity was gradually decreased with the increased amount of Au^{3+} (Figure 8B). The quenching constant was deduced to be 218670 M^{-1} from the Stern-Volmer plot of the relative PL intensity (I_0/I) versus the concentration of Au^{3+} ([Au^{3+}]) and the limit of detection (LOD) was thus calculated to be 6.5 ×10^{-7} M according to the equation of LOD = 3SB/m,[47] demonstrating high sensitivity of Au(III) detection (Figure 8C).

Excitingly, the precipitate was observed in THF/water mixture of **5** and Au^{3+} after 24 h at room temperature due to the poor solubility of the **5**-Au^{3+} complexes (Figure S11A), indicating that **5** could be utilized for the enrichment of Au^{3+} from aqueous solutions. As shown in Figure S11B, when the DMSO solution or solid powder of **5** (0.5 - 3 mg) were added into 8 mL of AuCl$_3$ solution (10 mg/L) and stirred at room temperature for 12 h, the precipitates of the complexes were readily formed, which were removed by centrifugation. The results of atom absorption spectroscopy (AAS) measurement of the remaining [Au^{3+}]in the filtrate indicated that both DMSO solution and solid powder of **5** could reduce [Au^{3+}] sharply with more than 99% enrichment efficiency. Moreover, the solid powder of **5** showed better performance than the DMSO solution of **5** in gold enrichment.

This gold extraction approach was hence applied to extract Au^{3+} directly from discarded computer processing units

(CPUs), whose metal scrap chippings were soaked in an aqueous solution of *N*-bromosuccinimide and pyridine,[44] to obtain a blue solution with 436.72 mg/L of Cu^{2+}, 115.06 mg/L of Ni^{2+}, and 10.40 mg/L of Au^{3+}. After the solution (8 mL) was treated with the solid powder of **5** (1 mg), The $[Au^{3+}]$ decreased significantly with the enrichment efficiency of 89.42% (Figure 8D, Table S4). On the contrary, the $[Ni^{2+}]$ and $[Cu^{2+}]$ remained almost intact with the enrichment efficiency of 1.91% and 1.79%, respectively, demonstrating that **5** could selectively extract Au^{3+} at practical condition in the presence of a high concentration of interference metal ions. It is worth noting that the extraction capacity of **5** is 475 mg·Au^{3+}/g, which is comparable to that of previous reports.[46]

The imidazolone derivative **5** was also found to be easily protonated (Figure S12). As shown in Figure 8E, a remarkable red shift in the emission of the filter paper containing **5**, which was fabricated by dripping the solution on it, was observed after exposed to HCl vapor. The emission maximum of the PL spectrum shifted from 557 to 621 nm, in turn, the fluorescence color changed from yellow to red accompanied with a large drop in intensity (Figure S13). Next, when the acid-treated **5** was exposed to ammonia vapor (NH_3) generated from its 0.08 M aqueous solution for only 5 s, the emission of **5** returned back to yellow. Notably, the yellow and red emission states could be interconverted for at least ten consecutive cycles with negligible fatigue, revealing the high reversibility and repeatability of this sensor system (Figure S14).

Besides ammonia can make the protonated **5** change color, biogenic amines, generated during the food spoilage process,[48,49] could work the same. Herein, the test strip of protonated **5** was investigated as the fluorescent sensor to detect *in situ* generated amines from food spoilage. The yellow croakers from seafood market were used as fresh detection samples. Two groups of yellow croakers were kept at room temperature and -18 °C, respectively (Figure 8F and G). No emission changes were observed when the test strips of protonated **5** were used to detect both two groups of yellow croakers at the beginning of time. After 24 h, only the test strip with the yellow croaker kept at room temperature showed emission change from red to yellow under UV irradiation. In this way, food spoilage sensors of **5** were established for sensitive and selective detection of ammonia and biogenic amines generated through the food spoilage process.

CONCLUSION

Linear and cross-linked poly(alkynoate)s **P1** and **P2** with excellent and visualized degradation are presented. **P1** could be successfully degraded by benzamidine **3** with 100% conversion into not only diols, a kind of monomers, but also high-value-added *N*-heterocyclic compounds **4** and **5** by altering the reaction conditions. Pyrimidone derivative **4** was obtained at 110 °C, whereas, imidazolone derivative **5** was obtained at 60 °C or at room temperature in the presence of catalyst Bu_3P. Thermoset poly(alkynoate) **P2** was also successfully degraded to imidazolone derivative **11**. The reaction kinetics and mechanism were well investigated via the *in situ* FT-IR spectroscopy and DFT calculation. The results showed that path B was observed with lower highest energy barrier than that of path A, but resulted in a more unstable product than that of path A, which indicated that only path B could occur at low temperature, meanwhile, path A is favored at elevated temperature with more stable products. PBu_3 could greatly reduce the energy barrier, so the reaction rate was increased immensely, which was also consistent with *in situ* FT-IR results.

It is worth noting that the first example of visualization of degradation process is realized by taking advantage of the AIE feature of the degraded products. Moreover, the degradation could occur on the polymer thin films, which could be introduced into μCP to generate fluorescence patterns. The *N*-heterocyclic compounds **4** and **5** obtained from **P1** possess show high added values. Pyrimidone derivative **4** could be applied in bioimaging and inhibiting bacteria. Meanwhile, imidazolone derivative **5** could be used for the detection and recovery of Au(III) ions from electronic waste and serve as the fluorescent sensor to detect *in situ* generated amines from food spoilage. Thus, this work presents a visualized and high value product-selective degradation to solve the end-of-life issue of polymers.

ASSOCIATED CONTENT

Supporting Information.
Experimental details, characterization data (DMA, FT-IR, NMR, UV, PL and AAS). This material is available free of charge via the Internet at http://pubs.acs.org.

AUTHOR INFORMATION

Corresponding Author

* msqinaj@scut.edu.cn (A.J.Q.)
* lingjun@zju.edu.cn (L.J.)
* tangbenz@ust.hk (B.Z.T.)

ACKNOWLEDGMENT

REFERENCES

(1) Ying, L.; Ho, C. L.; Wu, H.; Cao, Y.; Wong, W. Y. White polymer light-emitting devices for solid-state lighting: materials, devices, and recent progress. *Adv. Mater.* **2014**, *26*, 2459-2473.

(2) Wu, H.; Ying, L.; Yang, W.; Cao, Y. Progress and perspective of polymer white light-emitting devices and materials. *Chem. Soc. Rev.* **2009**, *38*, 3391-3400.

(3) Cui, C.; Li, Y. High-performance conjugated polymer donor materials for polymer solar cells with narrow-band gap nonfullerene acceptors. *Energy Environ. Sci.* **2019**, *12*, 3225-3246.

(4) Lee, C.; Lee, S.; Kim, G.-U.; Lee, W.; Kim, B. J. Recent advances, design guidelines, and prospects of all-polymer solar cells. *Chem. Rev.* **2019,** *119*, 8028-8086.

(5) Pollack, K. A.; Imbesi, P. M.; Raymond, J. E.; Wooley, K. L. Hyperbranched fluoropolymer-polydimethylsiloxane-poly (ethylene glycol) cross-linked terpolymer networks designed for marine and biomedical applications: heterogeneous nontoxic antibiofouling surfaces. *ACS Appl. Mater. Interfaces* **2014**, *6*, 19265-19274.

(6) (a) MacArthur, E. Beyond plastic waste. *Science* **2017**, *358*, 843; (b) Garcia, J. M.; Robertson, M. L. The future of plastics recycling. *Science* **2017**, *358*, 870-872.

(7) Wang, Z.; Ganewatta, M. S.; Tang, C. Sustainable polymers from biomass: Bridging chemistry with materials and processing. *Prog. Polym. Sci.* **2020**, *101*, 101197.

(8) Rahimi, A.; García, J. M. Chemical recycling of waste plastics for new materials production. *Nat. Rev. Chem.* **2017,** *1*, 46-57.

(9) Wang, H.; Su, L.; Li, R.; Zhang, S.; Fan, J.; Zhang, F.; Nguyen, T. P.; Wooley, K. L. Polyphosphoramidates that undergo acid-triggered backbone degradation. *ACS Macro Lett.* **2017**, *6*, 219-223.

(10) Hsu, T. G.; Zhou, J.; Su, H. W.; Schrage, B. R.; Ziegler, C. J.; Wang, J. A polymer with "locked" degradability: Superior backbone stability and accessible degradability enabled by mechanophore installation. *J. Am. Chem. Soc.* **2020**, *142*, 2100-2104.

(11) (a) Hong, M.; Chen, E. Y. X. Chemically recyclable polymers: a circular economy approach to sustainability. *Green Chem.* **2017,** *19*, 3692-3706; (b) Schneiderman, D. K.; Hillmyer, M. A. 50th anniversary perspective: There is a great future in sustainable polymers. *Macromolecules* **2017**, *50*, 3733-3749.

(12) Zhu, J. B.; Watson, E. M.; Tang, J.; Chen, E. Y. X. A synthetic polymer system with repeatable chemical recyclability. *Science* **2018**, *360*, 398-403.

(13) Tang, X.; Hong, M.; Falivene, L.; Caporaso, L.; Cavallo, L.; Chen, E. Y. X. The quest for converting biorenewable bifunctional alpha-methylene-gamma-butyrolactone into degradable and recyclable polyester: controlling vinyl-addition/ring-opening/cross-linking pathways. *J. Am. Chem. Soc.* **2016**, *138*, 14326-14337.

(14) Yuan, J.; Xiong, W.; Zhou, X.; Zhang, Y.; Shi, D.; Li, Z.; Lu, H. 4-Hydroxyproline-derived sustainable polythioesters: controlled ring-opening polymerization, complete recyclability, and facile functionalization. *J. Am. Chem. Soc.* **2019,** *141*, 4928-4935.

(15) Liu, Y.; Zhou, H.; Guo, J. Z.; Ren, W. M.; Lu, X. B. Completely recyclable monomers and polycarbonate: approach to sustainable polymers. *Angew. Chem. Int. Ed.* **2017**, *56*, 4862-4866.

(16) (a) Diesendruck, C. E.; Peterson, G. I.; Kulik, H. J.; Kaitz, J. A.; Mar, B. D.; May, P. A.; White, S. R.; Martinez, T. J.; Boydston, A. J.; Moore, J. S. Mechanically triggered heterolytic unzipping of a low-ceiling-temperature polymer. *Nat. Chem.* **2014**, *6*, 623-628; (b) Brutman, J. P.; De Hoe, G. X.; Schneiderman, D. K.; Le, T. N.; Hillmyer, M. A. Renewable, degradable, and chemically recyclable cross-linked elastomers. *Ind. Eng. Chem. Res.* **2016**, *55*, 11097-11106.

(17) Shi, C. X.; Guo, Y. T.; Wu, Y. H.; Li, Z. Y.; Wang, Y. Z.; Du, F. S.; Li, Z. C. Synthesis and controlled organobase-catalyzed ring-opening polymerization of morpholine-2,5-dione derivatives and monomer recovery by acid-catalyzed degradation of the polymers. *Macromolecules* **2019**, *52*, 4260-4269.

(18) Song, B.; He, B.; Qin, A.; Tang, B. Z. Direct polymerization of carbon dioxide, diynes, and alkyl dihalides under mild reaction conditions. *Macromolecules* **2018**, *51*, 42-48.

(19) Song, B.; Zhang, R.; Hu, R.; Chen, X.; Liu, D.; Guo, J.; Xu, X.; Qin, A.; Tang, B. Z., Site-selective, multistep functionalizations of CO_2-based hyperbranched poly(alkynoate)s toward functional polymetric materials. *Adv. Sci.* **2020**, 2000465.

(20) Song, B.; Qin, A.; Tang, B. Z. New polymerizations based on green monomer of carbon dioxide. *Acta Chim. Sinica* **2020**, *78*, 9-22.

(21) Song, B.; Qin, A. J.; Tang, B. Z. Green monomer of CO_2 and alkyne-based four-component tandem polymerization toward regio- and stereoregular poly(aminoacrylate)s. *Chinese J. Polym. Sci.* https://doi.org/10.1007/s10118-020-2454-2.

(22) Ruhemann, S.; Stapleton, H. E. The formation of heterocyclic compounds. *J. Chem. Soc.* **1900**, *77*, 239-244.

(23) Gabillet, S.; Loreau, O.; Specklin, S.; Rasalofonjatovo, E.; Taran, F. A phosphine-catalyzed preparation of 4-arylidene-5-imidazolones. *J. Org. Chem.* **2014**, *79*, 9894-9898.

(24) Ogden, W. A.; Guan, Z. Recyclable, strong, and highly malleable thermosets based on boroxine networks. *J. Am. Chem. Soc.* **2018**, *140*, 6217-6220.

(25) Marcus, R. A.; Rice, O. K. The kinetics of the recombination of methyl radicals and iodine atoms. *J. Phys. Chem.* **1951**, *55*, 894-908.

(26) Mei, J.; Leung, N. L.; Kwok, R. T.; Lam, J. W.; Tang, B. Z. Aggregation-induced emission: together we shine, united we soar! *Chem. Rev.* **2015,** *115*, 11718-11940.

(27) Yang, J.; Chi, Z.; Zhu, W.; Tang, B. Z.; Li, Z. Aggregation-induced emission: a coming-of-age ceremony at the age of eighteen. *Sci. China Chem.* **2019**, *62*, 1090-1098.

(28) Liu, B.; Pucci, A.; Baumgartner, T. Aggregation induced emission: a land of opportunities. *Mater. Chem. Front.* **2017**, *1*, 1689-1690.

(29) Robb, M. J.; Li, W.; Gergely, R. C.; Matthews, C. C.; White, S. R.; Sottos, N. R.; Moore, J. S. A robust damage-reporting strategy for polymeric materials enabled by aggregation-induced emission. *ACS Central Sci.* **2016**, *2*, 598-603.

(30) Ye, X.; Liu, Y.; Lv, Y.; Liu, G.; Zheng, X.; Han, Q.; Jackson, K. A.; Tao, X. *In situ* microscopic observation of the crystallization process of molecular microparticles by fluorescence switching. *Angew. Chem. Int. Ed.* **2015**, *54*, 7976-7980.

(31) Song, Z.; Lv, X.; Gao, L.; Jiang, L. Dramatic differences in the fluorescence of AIEgen-doped micro-and macrophase separated systems. *J. Mater. Chem. C* **2018**, *6*, 171-177.

(32) Liu, S.; Cheng, Y.; Zhang, H.; Qiu, Z.; Kwok, R. T. K.; Lam, J. W. Y.; Tang, B. Z. *In situ* monitoring of RAFT polymerization by tetraphenylethylene-containing agents with aggregation-induced emission characteristics. *Angew. Chem. Int Ed.* **2018,** *57*, 6274-6278.

(33) Qiu, Z.; Zhao, W.; Cao, M.; Wang, Y.; Lam, J. W.; Zhang, Z.; Chen, X.; Tang, B. Z. Dynamic visualization of stress/strain distribution and fatigue crack propagation by an organic mechanoresponsive AIE luminogen. *Adv. Mater.* **2018**, *30*, 1803924.

(34) (a) Borowiec, J.; Hampl, J.; Singh, S.; Haefner, S.; Friedel, K.; Mai, P.; Brauer, D.; Ruther, F.; Liverani, L.; Boccaccini, A. R. 3D microcontact printing for combined chemical and topographical patterning on porous cell culture membrane. *ACS Appl. Mater. Interfaces* **2018**, *10*, 22857-22865; (b) Buten, C.; Lamping, S.; Körsgen, M.; Arlinghaus, H. F.; Jamieson, C.; Ravoo, B. J. Surface functionalization with carboxylic acids by photochemical microcontact printing and tetrazole chemistry. *Langmuir*, **2018**, *34*, 2132-2138.

(35) Kyvik, A. R.; Luque-Corredera, C.; Pulido, D.; Royo, M.; Veciana, J.; Guasch, J.; Ratera, I. Stimuli-responsive functionalization strategies to spatially and temporally control surface properties: michael vs diels–alder type additions. *J. Phys. Chem. B* **2018**, *122*, 4481-4490.

(36) Spruell, J. M.; Sheriff, B. A.; Rozkiewicz, D. I.; Dichtel, W. R.; Rohde, R. D.; Reinhoudt, D. N.; Stoddart, J. F.; Heath, J. R. Heterogeneous catalysis through microcontact printing. *Angew. Chem. Int. Ed.* **2008**, *47*, 9927 –9932.

(37) Wendeln, C.; Rinnen, S.; Schulz, C.; Kaufmann, T.; Arlinghaus, H. F.; Ravoo, B. J. Rapid preparation of multifunctional surfaces for orthogonal ligation by microcontact chemistry. *Chem. Eur. J.* **2012**, *18*, 5880-5888.

(38) Wagner, E.; Becan, L.; Nowakowska, E. Synthesis and pharmacological assessment of derivatives of isoxazolo [4,5-d] pyrimidine. *Bioorgan. Med. Chem.* **2004**, *12*, 265-272.

(39) Xue, H.; Zhao, Y.; Wu, H.; Wang, Z.; Yang, B.; Wei, Y.; Wang Z.; Tao, L. Multicomponent combinatorial polymerization via the Biginelli reaction. *J. Am. Chem. Soc.* **2016**, *138*, 8690-8693.

(40) Zhao, Y.; Wu, H.; Wang, Z.; Wei, Y.; Wang, Z.; Tao, L. Training the old dog new tricks: the applications of the Biginelli reaction in polymer chemistry. *Sci. China Chem.* **2016**, *59*, 1541-1547.

(41) Puddephatt, R. J. Macrocycles, catenanes, oligomers and polymers in gold chemistry. *Chem. Soc. Rev.* **2008**, *37*, 2012-2027.

(42) Zeng, X.; Mathews, J. A.; Li, J. Urban mining of E-waste is becoming more cost-effective than virgin mining. *Environ. Sci. Technol.* **2018**, *52*, 4835-4841.

(43) Sun, D. T.; Gasilova, N.; Yang, S.; Oveisi, E.; Queen, W. L. Rapid, selective extraction of trace amounts of gold from com-

plex water mixtures with a metal-organic framework (MOF)/polymer composite. *J. Am. Chem. Soc.* **2018,** *140*, 16697-16703.

(44) Yue, C.; Sun, H.; Liu, W.-J.; Guan, B.; Deng, X.; Zhang, X.; Yang, P. Environmentally benign, rapid, and selective extraction of gold from ores and waste electronic materials. *Angew. Chem., Int. Ed.* **2017**, *56*, 9331-9335.

(45) Sun, D. T.; Peng, L.; Reeder, W. S.; Moosavi, S. M.; Tiana, D.; Britt, D. K.; Oveisi E.; Queen, W. L. Rapid, selective heavy metal removal from water by a metal–organic framework/polydopamine composite. *ACS Central Sci.* **2018**, *4*, 349-356.

(46) Cao, W.; Dai, F.; Hu, R.; Tang, B. Z. Economic sulfur conversion to functional polythioamides through catalyst-free multicomponent polymerizations of sulfur, acids, and amines. *J. Am. Chem. Soc.* **2019**, *142*, 978-986.

(47) Deng, H. M.; Huang, L. J.; Chai, Y. Q.; Yuan, R.; Yuan, Y. L. Ultrasensitive photoelectrochemical detection of multiple metal ions based on wavelength-resolved dual-signal output triggered by click reaction. *Anal. Chem.* **2019**, *91*, 2861-2868.

(48) Apetrei, I. M.; Apetrei, C. Application of voltammetric e-tongue for the detection of ammonia and putrescine in beef products. *Sensors Actuat. B-Chem.* **2016**, *234*, 371-379.

(49) Mackin, C.; Schroeder, V.; Zurutuza, A.; Su, C.; Kong, J.; Swager, T. M.; Palacios, T. Chemiresistive graphene sensors for ammonia detection. *ACS Appl. Mater. Interfaces* **2018**, *10*, 16169-16176.

Table of Content